Ultrastrong coupling of vibrationally dressed organic Frenkel excitons with Bloch surface waves in a one-sided all-dielectric structure

Shaocong Hou, Yue Qu, Xiao Liu, and Stephen R. Forrest

Phys. Rev. B **100**, 045410 — Published 15 July 2019

DOI: 10.1103/PhysRevB.100.045410

Ultrastrong coupling of vibrationally dressed organic Frenkel excitons with Bloch surface waves in a one-sided all-dielectric structure

Shaocong Hou[1, †], Yue Qu[1, †], Xiao Liu[1], Stephen R. Forrest[1,2,3]

[†] These authors contributed equally to this work

[1] Department of Electrical Engineering and Computer Science, University of Michigan, Ann Arbor, MI 48109, USA

[2] Department of Physics, University of Michigan, Ann Arbor, MI 48109, USA

[3] Department of Materials Science and Engineering, University of Michigan, Ann Arbor, MI 48109, USA

Abstract

We demonstrate a transition from weak, to strong, to ultrastrong coupling of Frenkel molecular excitons and Bloch surface wave photons at room temperature using a one-sided, all-dielectric optical structure. The all-dielectric structure comprises an organic semiconductor thin film on the surface of a distributed Bragg reflector. We investigate the evolution of multiple vibronic polariton branches and their dominant absorption peaks as a function of coupling and in-plane momentum, which is absent in previous ultrastrong coupling systems. Measurements are interpreted using both the transfer matrix method and a coupled-oscillator model without rotating wave approximation. The dependence of Rabi splitting on the number of excitons and electrical field amplitude is also modeled showing a transition to ultrastrong coupling at film thicknesses $\geq$50 nm. This low-loss polaritonic structure enables to study phenomena, such as organic exciton-polariton dynamics, ultralong range polariton propagation and high efficiency energy transport, in the ultrastrong coupling regime at room temperature.

Introduction

Exciton-polaritons are hybrid quasiparticles arising from strong coupling of excitons and photons when their coupling strength (g) is larger than individual damping rates of excitons (γ_{ph}) and photons (γ_{ex}). Early observations of strong coupling of photons and Wannier-Mott excitons in inorganic semiconductors required high-quality factor (Q) dielectric microcavities at cryogenic temperatures. This was necessitated due to their small vacuum Rabi splitting energies ($\hbar\Omega \approx 2\hbar g$, where $\hbar$ is reduced Plank's constant) and small exciton binding energies of a few to tens of meV. In contrast, large Rabi splittings in disordered organic semiconductors are observed at room temperature due to high oscillator strengths and large Frenkel exciton binding energies. [1] When the Rabi splitting energy is nominally $\geq$10% of the uncoupled Frenkel exciton energy ($\hbar g \geq 0.1\hbar\omega_{ex}$), the ultrastrong coupling regime is reached. Exploration of this regime offers opportunities to investigate interesting quantum electrodynamics and nonlinear optical properties of organic materials.[2,3] Low-Q metallic cavities or surface plasmonic modes are commonly used to confine the optical field to induce ultrastrong coupling with a maximum coupling ratio of $g/\omega_{ex} = 0.31$. [4–10] However, metal cavities suffer from significant optical losses, thereby defeating many of the inherent advantages, such as long-range transport and optical nonlinearities found in this regime. All-dielectric structures with reduced loss are therefore desirable, but to our knowledge have yet to be realized.

In this work, we show ultrastrong exciton-photon coupling in a one-sided structure comprising a distributed Bragg reflector (DBR) supporting a low-loss Bloch surface wave (BSW) [11–15] coated with a tetraphenyldibenzoperiflanthene (DBP) thin film (Fig. 1a inset).

Multiple exciton-polariton branches with vibronic features are observed in both the strong and ultrastrong coupling regimes, and the separation between dominant absorptive polariton branches increases with coupling strength. The measurements are interpreted using transfer matrix simulations and a coupled-oscillator model without rotating wave approximation. We analyze the coupling strengths and quantify their dependence on the number of absorbers and the electric field strength. This low-loss polaritonic structure enable long range exciton-polariton transport and high efficiency energy transfer in an ultrastrong coupling regime at room temperature.

Theory

The rotating-wave approximation commonly used to describe strong coupling is not applicable in the ultrastrong regime. A full Hamiltonian containing both diamagnetic and anti-resonant terms is thus employed: [10]

$$H = \hbar \sum_q \sum_n \omega_{cav,q} \left(a_q^\dagger a_q + \frac{1}{2} \right) + \omega_{ex,n} \left(b_{q,n}^\dagger b_{q,n} + \frac{1}{2} \right)$$
$$+ \hbar \sum_q \sum_n D_q \left(a_q^\dagger a_q + a_q a_q^\dagger \right) + i g_q \left(a_q^\dagger b_{q,n} + b_q^\dagger a_{q,n} \right)$$
$$+ \hbar \sum_q \sum_n D_q \left(a_q a_{-q} + a_q^\dagger a_{-q}^\dagger \right) + i g_q \left(a_q b_{-q,n} + a_q^\dagger b_{-q,n}^\dagger \right) \quad (1)$$

where q is the in-plane wavevector, $a^\dagger(a)$ and $b^\dagger(b)$ are creation (annihilation) operators for photons at energy $\hbar\omega_{cav}$ and a number n of excitons at energy $\hbar\omega_{ex,n}$, and D_q is the diamagnetic coupling constant. For one photon and three exciton oscillators (corresponding to the 0-0, 0-1 and 0-2 vibronic states of DBP), the 8 × 8 Hamiltonian matrix M is:

$$\begin{bmatrix} \omega_{ph}+\frac{2D}{\hbar} & -ig_1 & -ig_2 & -ig_3 & -\frac{2D}{\hbar} & -ig_1 & -ig_2 & -ig_3 \\ ig_1 & \omega_{ex1} & 0 & 0 & -ig_1 & 0 & 0 & 0 \\ ig_2 & 0 & \omega_{ex2} & 0 & -ig_2 & 0 & 0 & 0 \\ ig_3 & 0 & 0 & \omega_{ex3} & -ig_3 & 0 & 0 & 0 \\ \frac{2D}{\hbar} & -ig_1 & -ig_2 & -ig_3 & -\omega_{cav}-\frac{2D}{\hbar} & -ig_1 & -ig_2 & -ig_3 \\ -ig_1 & 0 & 0 & 0 & ig_1 & -\omega_{ex1} & 0 & 0 \\ -ig_2 & 0 & 0 & 0 & ig_2 & 0 & -\omega_{ex2} & 0 \\ -ig_3 & 0 & 0 & 0 & ig_3 & 0 & 0 & -\omega_{ex3} \end{bmatrix} \quad (2)$$

where g_1, g_2, g_3 are the coupling strengths between the photon and three excitons, and $D \approx \sum_{i=1,2,3} \frac{{g_i}^2}{\omega_{ex,i}}$. Its eigenvector ($\alpha$, β_1, β_1, β_1, x, y_1, y_2, y_3)^T contains Hopfield coefficients of the photon, three excitons and their virtual contributions.

Results

A DBR consisting of 6 pairs of 100 nm thick SiN_x and 135 nm thick SiO_2 capped by 10 nm thick SiN_x and 15 nm thick SiO_2 layers were deposited by plasma enhanced chemical vapor deposition on a fused silica substrate. This was followed by depositing DBP films with different thicknesses (d = 2 nm to 50 nm), by vacuum thermal evaporation. Three well-resolved absorption peaks of DBP are shown in Fig. 1a. Optical constants of DBP were measured by spectroscopic ellipsometry and fitted with a Gaussian oscillator model yielding three exciton resonance energies of $\hbar\omega_{ex,i}$ = 2.04 eV, 2.22 eV and 2.38 eV (i =1, 2, 3) corresponding to the vibronic progression 0-0, 0-1 and 0-2, respectively. The full width at half maxima (FWHM) were $\Gamma_{1\text{-}3}$ = 133 meV, 141 meV and 147 meV, the relative oscillator strengths were $f_1 : f_2 : f_3$ = 1:0.82:0.39, and the background dielectric constant [16] was ε_∞ = 3.0. The Kretschmann configuration was used in the angle-resolved reflectivity measurements to observe the polaritons

with the DBP layer capping the DBR. A glass prism was attached to the substrate using index-matching fluid (refractive index n = 1.5), as shown in Fig. 1b.

To extract the coupling-strengths between excitons and photons, BSW dispersion relations with different DBP layer thicknesses (d) are calculated using transfer matrix simulations. The calculation uses an equivalent organic layer on top of the DBR with the background dielectric constant of DBP. This "equivalent organic layer" intentionally eliminates exciton characteristics to allow for modelling of optical mode alone. A transverse electric (TE) polarized BSW mode is supported by the DBR and confined to a small volume (~λ/4, λ being the resonant wavelength), with the field intensity peak just beneath the organic layer (Fig. 1c). Figure 1d shows the simulated BSW dispersion relation of the DBR capped with a DBP layer with d = 50 nm. For comparison, the dispersion relation of the DBR with a free top surface (black line: simulation, open circles: measurement) is also shown. Compared with the free surface DBR (d = 0 nm), the BSW on the DBR capped with DBP (red line) exhibits a red-shifted energy cutoff, and the dispersion relation is perturbed by partial hybridization with the guided modes, consistent with previous reports. [17] Both open cavities showed narrow resonance dips centered at 2.04 eV (Fig. 1d, inset), and a calculated $Q \sim 10^3$.

The TE reflectivity spectra of a 30 nm (left) and 50 nm (right) thick DBP-loaded DBR above the total internal reflection angle are simulated, as shown in Figs. 2a and b. Four branches (guided by red dashed lines) between 1.6 eV and 2.5 eV are separated from three uncoupled vibronic states 0-0, 0-1, 0-2 (indicated by vertical dashed lines from left to right). All of the predicted features are readily distinguished in the prism-coupled measurements in Fig. 2c and d.

The low reflectivity below 1.6 eV or above 2.5 eV is due to the DBR stop band and absorption of SiN_x and the broadening is primarily due to the angular spread of the prism coupled beam as well as the limited angular resolution of our setup. At all angles, the lowest-energy reflectivity dip is relatively strong and narrow, and it shifts to higher energy with increasing angle. Other dips are relatively weak and broad. The energy of the dip between the 0-0 and 0-1 vibronics is independent of angle, while that of the dip between 0-1 and 0-2 increases slightly with angle. The highest-energy dip (above the 0-2 transition) emerges above 46^o and blue shifts with increasing angle. For all simulations, the contrast in reflectivity is small, especially at high angles.

The reflectivity minima of the measured spectra of the 50 nm-thick sample are extracted assuming a Gaussian lineshape and are plotted in Fig. 3a. The lower (LP), first middle (MP1), second middle (MP2) and upper (UP) branches are observed with anti-crossing features near three uncoupled exciton resonant energies (three horizontal dashed lines), a signature of exciton-photon coupling. Large splitting observed between LP and MP1 indicates a large coupling strength and thus g/ω_{ex} ratio, probably leading to an invalidation of rotating-wave approximation.

Discussion

To estimate coupling strengths and vacuum Rabi splitting energies, we fit the measured data with the 8 × 8 Hamiltonian matrix, where the uncoupled photon energy ($\hbar\omega_{ph}$) is calculated using the transfer matrix method, and the several vibronic transitions are treated as individual exciton states. [18] The least-squares fit yields coupling strengths of $\hbar g_1 = 205$ meV, $\hbar g_2 = 177$ meV, and

$\hbar g_3$ = 136 meV. Using a photon linewidth of Γ_{cav} = 5 meV, and an exciton width Γ_{ex} = 133 meV, the vacuum Rabi splitting energy is:

$$\hbar\Omega_i = \sqrt{4\hbar g_i^2 - \left(\Gamma_{ex} - \Gamma_{ph}\right)^2} \qquad (i = 1, 2, 3) \tag{3}$$

The extracted Rabi splitting energies $\hbar\Omega_1$ = 389 meV, $\hbar\Omega_2$ = 329 meV, $\hbar\Omega_3$ = 238 meV are larger than spectral widths of uncoupled photon and exciton states. Thus, $g_1/\omega_{ex,1} \approx 0.1$ confirms ultrastrong coupling regime has been reached. The Hopfield coefficients of LP are shown in Figure 3b. Similar fitting for samples with thicknesses of 3 - 40 nm (not shown here) indicate that they do not reach the ultrastrong coupling regime.

In the ultrastrong regime, the virtual contributions to the polariton ground state cannot be ignored. The virtual photon content ($|x_{LP}|^2+|x_{MP1}|^2+|x_{MP2}|^2+|x_{UP}|^2$) and virtual exciton contributions ($|y_{i,LP}|^2+|y_{i,MP1}|^2+|y_{i,MP2}|^2+|y_{i,UP}|^2$) are calculated and shown in Fig. 3c. The virtual photon content is approximately 0.55% per state, and the contents of virtual excitons 0-0, 0-1 and 0-2 are 0.2%, 0.15%, and 0.1% to the ground state, respectively.

The Rabi splitting energy ($\hbar\Omega_1$) monotonically increases with DBP layer thickness as shown in Fig. 4a. The coupling strength is increased with $\sqrt{N}$, where N is the number of molecules, which is proportional to organic layer thickness, d. Thus, the Rabi splitting energy is fit using $\hbar\Omega(d) = A\sqrt{d - d_0}$, shown as the dashed line, where A is a constant, and d_0 is the critical DBP thickness demarking the transition from weak to strong coupling. Although thin DBP samples with d < 15 nm can be fit by this expression, a slower increase in $\hbar\Omega(d)$ is observed at greater thickness. This deviation results from the exponential attenuation in electric field with distance from the DBR surface, as shown in Fig. 1c. To account for the reduction in

field intensity with distance, we integrate over the film thickness *viz.*:

$$\hbar\Omega(d) \propto 2\mu\sqrt{N}\bar{E} = 2\mu\sqrt{N}\int_0^d \frac{e^{-x/l}}{d}dx = A'\frac{1-e^{-\frac{d-d_0}{l}}}{\sqrt{d-d_0}} \quad (4)$$

where the characteristic field decay length is l, μ is molecular transition dipole moment, and A', d_0 and l are fitting parameters. A fit to this expression is indicated by the solid line in Fig. 4a.

It is interesting to study the energy shift of the polariton branches and their absorption as the coupling strength becomes comparable with the vibrational frequency ($g \sim \omega_v$). [19,20] Figure 4b shows the simulated reflectivity of samples with different organic layer thicknesses, namely with different coupling strengths between 0-0 excitons and BSW photons. The angle for each thickness is chosen such that the BSW photon is resonant with the 0-0 exciton-photon. With larger coupling strengths, all polariton branches detune from the exciton energies except for MP1, that remains constant when g_1 is comparable with the phonon energy. As the coupling strength increases, the most intense polariton absorption remains located at the lowest branch, while the dominant polariton absorption at the higher energy side shifts from MP1 to MP2 and UP. This trend can also be found in the experimental reflectivity spectrum.

Conclusions

Ultrastrong coupling of Frenkel excitons and BSW photons is demonstrated in an all-dielectric, one-sided photonic structure. It is striking that in this ultrastrong regime, we still observe reflectivity from the middle vibronic polariton branches. Using a coupled-oscillator model, coupling strengths as large as 205 meV ($\hbar\Omega_1$ = 389 meV) are extracted, corresponding to $g/\omega_{ex} \approx 0.1$. We analyze the thickness dependence of the reflectivity spectra and find that the

coupling strength is tuned by balancing the layer thickness with the electric field amplitude at the surface of the DBR. The evolution of vibronic polariton branches shows that the dominant polariton branches diverge with increasing coupling strength. The all-dielectric structure extends the application space available to investigate polariton physics, such as ultralong-range polariton propagation, energy transfer and nonlinear optical effects in the ultrastrong regime.

Acknowledgments

We acknowledge Jongchan Kim, Kan Ding and Caleb Coburn for helpful discussions. This work is partially supported by the U.S. Department of Energy, Office of Science under Award Number DE-SC0017971 (SCH and XL, experiment, analysis, manuscript preparation, SRF, analysis and manuscript preparation), and the Air Force Office of Scientific Research, Award Number 17RT0908 (YQ, analysis and manuscript preparation) .

Reference

[1] D. Lidzey, D. Bradley, M. Skolnick, T. Virgili, S. Walker, and D. Whittaker, Nature **395**, 53 (1998).

[2] P. Forn-Díaz, L. Lamata, E. Rico, J. Kono, and E. Solano, ArXiv Prepr. ArXiv1804.09275 (2018).

[3] A. F. Kockum, A. Miranowicz, S. De Liberato, S. Savasta, and F. Nori, Nat. Rev. Phys. **1**, (2018).

[4] T. Schwartz and T. W. Ebbesen, Phys. Rev. Lett. **106**, 196405 (2011).

[5] S. Balci, Opt. Lett. **38**, 4498 (2013).

[6] S. Kéna-Cohen, S. A. Maier, and D. D. C. Bradley, Adv. Opt. Mater. **1**, 827 (2013).

[7] F. Barachati, J. Simon, Y. A. Getmanenko, S. Barlow, S. R. Marder, and S. Kéna-Cohen, ACS Photonics **5**, 119 (2018).

[8] A. Cacciola, O. Di Stefano, R. Stassi, R. Saija, and S. Savasta, ACS Nano **8**, 11483 (2014).

[9] M. Held, A. Graf, Y. Zakharko, P. Chao, L. Tropf, M. C. Gather, and J. Zaumseil, Adv. Opt. Mater. **6**, 1700962 (2018).

[10] F. Le Roux and D. D. C. Bradley, Phys. Rev. B **98**, 1 (2018).

[11] M. Liscidini, D. Gerace, D. Sanvitto, and D. Bajoni, Appl. Phys. Lett. **98**, 121118 (2011).

[12] S. Pirotta, M. Patrini, M. Liscidini, M. Galli, G. Dacarro, G. Canazza, G. Guizzetti, D.

Comoretto, and D. Bajoni, Appl. Phys. Lett. **104**, 51111 (2014).

[13] F. Barachati, A. Fieramosca, S. Hafezian, J. Gu, B. Chakraborty, D. Ballarini, L. Martinu, V. Menon, D. Sanvitto, and S. Kéna-Cohen, Nat. Nanotechnol. **13**, 906 (2018).

[14] S. Pirotta, M. Patrini, M. Liscidini, M. Galli, G. Dacarro, G. Guizzetti, D. Comoretto, and D. Bajoni, Opt. Lett. **39**, 2068 (2014).

[15] G. Lerario, D. Ballarini, A. Fieramosca, A. Cannavale, A. Genco, F. Mangione, S. Gambino, L. Dominici, M. De Giorgi, G. Gigli, and D. Sanvitto, Light Sci. Appl. **6**, e16212 (2017).

[16] V. M. Agranovich, *Excitations in Organic Solids* (OUP Oxford, 2009).

[17] R. Wang, H. Xia, D. Zhang, J. Chen, L. Zhu, Y. Wang, E. Yang, T. Zang, X. Wen, G. Zou, P. Wang, H. Ming, R. Badugu, and J. R. Lakowicz, Nat. Commun. **8**, (2017).

[18] R. J. Holmes and S. R. Forrest, Phys. Rev. Lett. **93**, 1 (2004).

[19] F. Herrera and F. C. Spano, Phys. Rev. Lett. **118**, 1 (2017).

[20] M. A. Zeb, P. G. Kirton, and J. Keeling, ACS Photonics **5**, 249 (2018).

Figure Captions

Figure 1. (a) Absorption spectrum of DBP. Absorption peaks of the 0-0, 0-1 and 0-2 vibronic transitions are indicated by vertical dashed lines. *Inset*: DBP molecular structure. b) Schematic of the one-sided optical cavity capped by DBP. The right-angle prism is used for optical coupling to the DBR capped by a d nm thick DBP organic layer. The measurement angle is θ. c). Simulated transverse electric (TE) optical field intensity profile of the Bloch surface wave (BSW) with a 30 nm DBP layer. d) Calculated dispersion relation of the BSW mode without (d = 0 nm) and with a 50 nm-thick DBP layer. Open circles show the measured dispersion of the bare cavity.

Figure 2. Simulated TE-polarized reflectivity spectra of a (a) d = 30 nm thick DBP layer on a DBR at incidence angles of 41.7^o, 44.3^o, 45.7^o, 47.7^o, 50.3^o, 51.6^o and (b) d = 50 nm thick DBP layer on a DBR at incidence angles of 44.3^o, 45.7^o, 47^o, 47.6^o, 48.3^o, 49^o, 49.6^o, 50.9^o (curves from bottom to top). Measurements corresponding to (a) and (b) are shown in (c) and (d), respectively. Red dashed lines provide guides for the polariton branches; vertical black dashed lines indicate the uncoupled exciton energies. Four polariton branches are observed from low to high energy: the lower (LP), first middle (MP1), second middle (MP2), and upper polariton branch (UP).

Figure 3. Dispersion relations of BSW-exciton polaritons in the ultrastrong-coupling

regime (d = 50 nm). (a) Least-squares fit (solid lines) to data (circles) of the angle-dependent reflectivity minima. The fits assume three coupled oscillators with coupling strengths of g_1 = 205 meV, g_2 = 177 meV, and g_3 = 136 meV. Colored horizontal dashed lines are guides for the uncoupled 0-0, 0-1, 0-2 exciton energies; black dashed line: calculated dispersion of the BSW photon (Ph). (b) Hopfield coefficients of LP: photon (black line) and three excitons (colored lines). (c) Virtual photon (black) and exciton (colored) content of the polariton ground state (GS).

Figure 4. (a) Vacuum Rabi splitting energy vs. DBP thickness. Dots are the extracted vacuum Rabi splitting energies ($\hbar\Omega_1$). The dashed line is a fit to the constant field approximation. The solid line accounts for field attenuation, with fitting parameters A' = 4.45±0.50 eV, l = 53 ± 8 nm, and d_0 = 2.9 ± 0.8 nm. (b) Simulated reflectivity of samples with d = 2, 5, 10, 15, 25, 30, 40, and 50 nm (curves from bottom to top) at angles corresponding to $|\omega_{cav} - \omega_{ex1}|$ = 0. Blue dashed line is a guide for the evolution of low-energy absorption peak, and red dashed lines guide for the high-energy absorption peak as coupling strength increases.

Figure 1

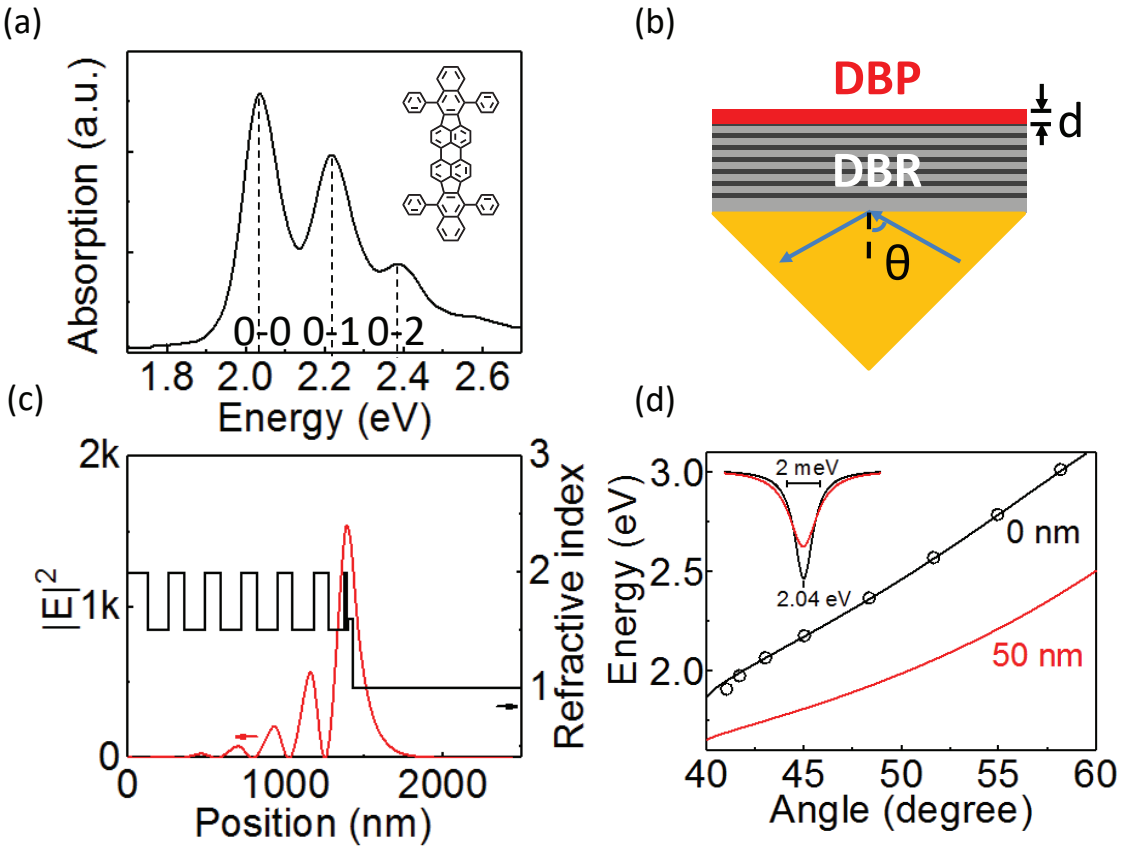

Figure 1 LB16596B 26JUN2019

Figure 2

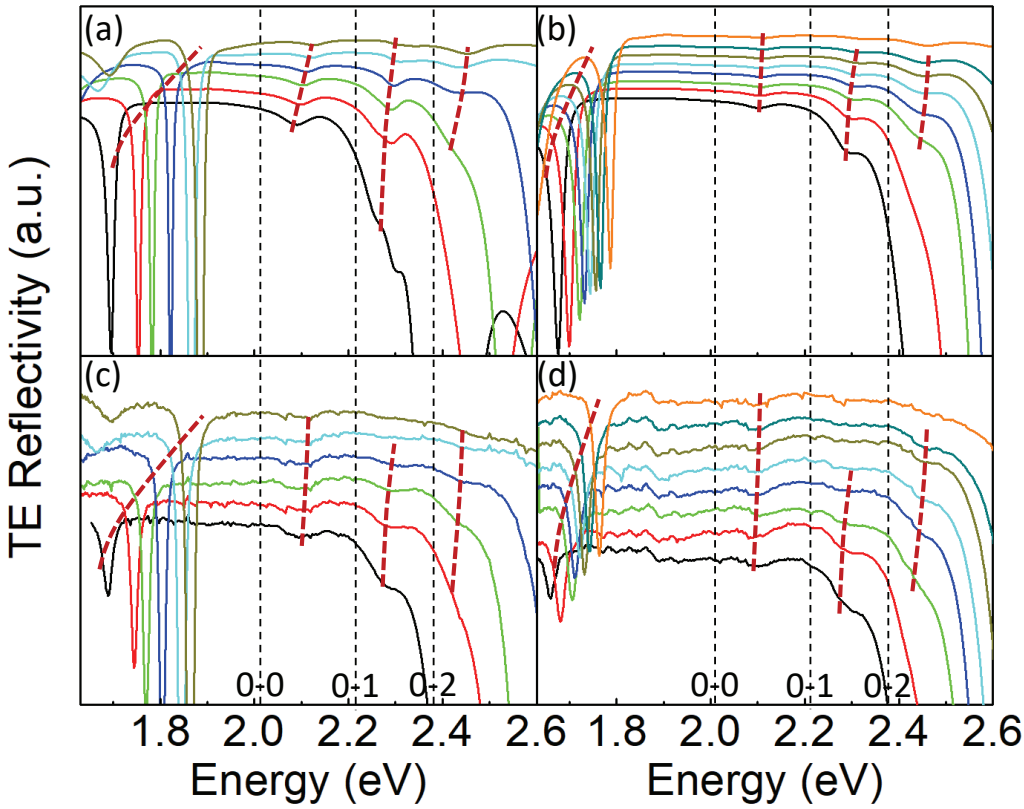

Figure 2 LB16596B 26JUN2019

Figure 3

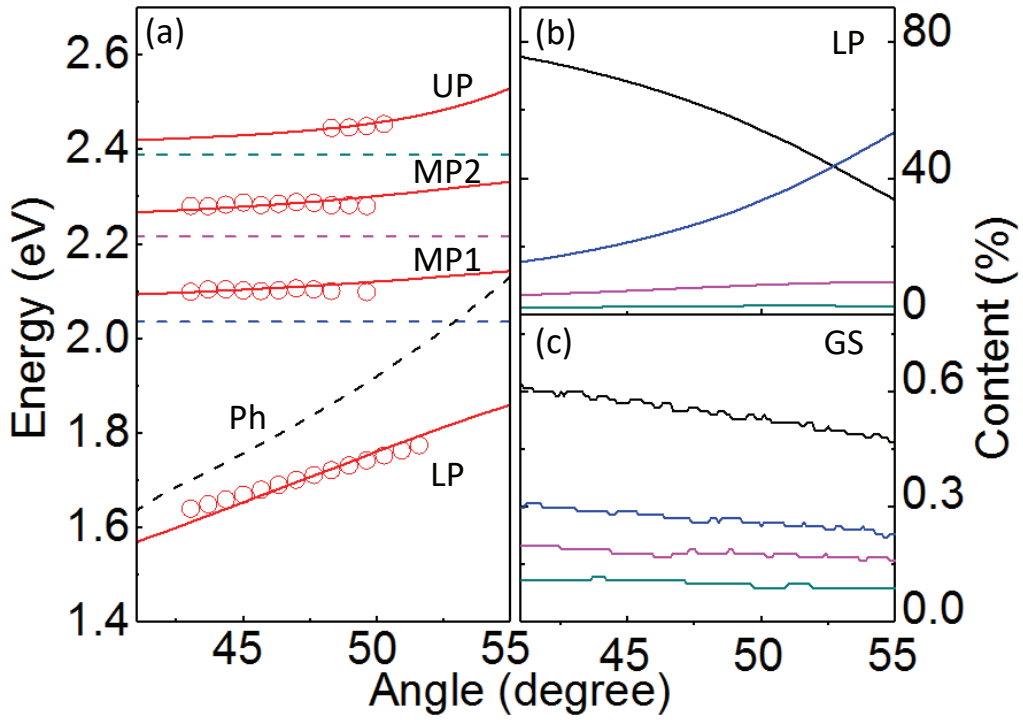

Figure 3 LB16596B 26JUN2019

Figure 4

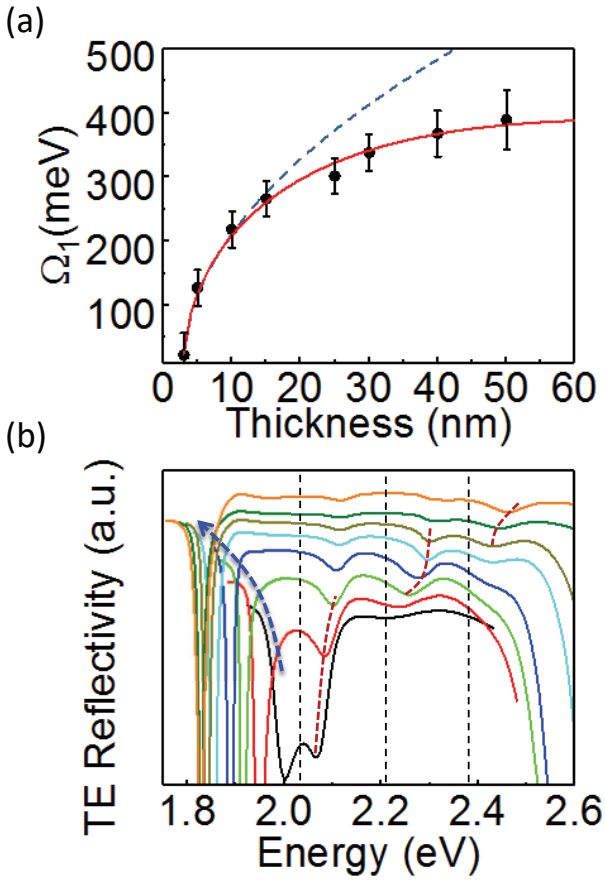

Figure 4 LB16596B 26JUN2019